Ninth 1International Conference on CFD in Minerals and Process Industries
CSIRO, Melbourne Australia
10-12 December 2012

FULLY RESOLVED SIMULATION OF FLOWS WITH NON-SPHERICAL PARTICLES USING AN IMMERSED BOUNDARY METHOD

S.H.L. KRIEBITZSCH*, M.A. van der HOEF and J.A.M. KUIPERS

Multiphase Reactors, Department of Chemical Engineering and Chemistry, Eindhoven University of Technology,
P.O. Box 513, 5600 MB Eindhoven, THE NETHERLANDS
*Corresponding author, E-mail address: S.H.L.Kriebitzsch@tue.nl

ABSTRACT

In this paper we present results of fully resolved simulations of gas-flows with non-spherical particles. To this end an in-house immersed-boundary CFD code for the simulation of spherical particles has been extended to allow for the simulation of sphero-cylindrical particles. Fully resolved simulations are limited to study small model systems, however such numerical experiments are a valuable method to improve our fundamental understanding of the behaviour of granular systems or to validate and improve larger scale models. Here, we compute the flow in periodic static random arrays of particles for different aspect ratios of the sphero-cylinders. Results for the drag force are compared with available literature data for spherical and non-spherical particles. First results for low Reynolds number flows indicate that a Carman-Kozeny description, where the drag force is determined solely by the hydraulic radius is still valid.

Keywords: drag force, immersed boundary, DNS

NOMENCLATURE

A, B	Fitting coefficients in the generalized Ergun equation $[-]$
d	Diameter of the volume-equivalent sphere [m]
D	Diameter of the cylinder [m]
F	Dimensionless drag force, defined as the ratio of actual drag to the Stokes drag $[-]$
$\boldsymbol{F}_{g\rightarrow s}$	Total gas-solid interaction force [N]
$\boldsymbol{F}^{\mathrm{IB}}$	Immersed boundary force computed at the Lagrangian marker points [N]
$\boldsymbol{f}^{\mathrm{IB}}$	Immersed boundary force density as defined on the Eulerian grid for the fluid $[\frac{\mathrm{N}}{\mathrm{m}^3}]$
F_{L}	Force per unit length normalized by $4\pi\,\mu\boldsymbol{U}$ $[-]$
F_{SC}	Dimensionless drag force in a simple cubic array $[-]$
F_{∞}	Dimensionless drag force on a cylinder in an unbounded fluid $[-]$
h	Grid size used in the simulations [m]
L	Length of the cylinder [m]
P	Fluid phase pressure [Pa]
Re	Particle Reynolds number: $Re = \frac{\rho_G d_{\mathrm{P}} \boldsymbol{U}}{\mu}$ $[-]$
r_h	Hydraulic radius of the pores in a porous medium [m]
S_{P}	Surface area of a particle [m^2]
$\boldsymbol{U}$	Mean relative superficial velocity $[\frac{\mathrm{m}}{\mathrm{s}}]$
$\boldsymbol{u}$	Fluid velocity $[\frac{\mathrm{m}}{\mathrm{s}}]$
V_{P}	Volume of a particle [m^3]
x	Aspect ratio of the cylinder: $\frac{L}{D}$ $[-]$
Δt	Time step used in the simulations [s]
ϕ	Solids volume fraction $[-]$
κ	Permeability of a random array [m^2]
μ	Dynamic viscosity of the gas phase [Pa s]
ψ	Sphericity of the particle $\frac{\pi d^2}{\pi DL}$ $[-]$
ρ_G	Density of the fluid phase $[\frac{\mathrm{kg}}{\mathrm{m}^3}]$
ξ	Ratio of d and D: $\frac{d}{D}$ $[-]$

INTRODUCTION

Numerical simulations are a ready means to study the flow in gas-solid fluidized bed. Detailed information on both phases, e.g. the velocity field of gas- and solids-phase, are obtained simultaneously which is difficult if not impossibleto achieve in experiments. However coarsened models, such as the Two-Fluid Model (TFM) or the Discrete-Particle Model (DPM), have to be used to perform computations in geometries comparable to lab or pilot scale (van der Hoef et al., 2008). In these models typically a spherical shape of the particle is assumed, as this allows to model the particle-particle interaction based on the kinetic theory of granular flow in case of TFM, or simplifies the collision detection in case of DPM. Only a few studies exist that include non-spherical particle shape into DPM type simulations in dry granular flow (e.g. Vu-Qouc et al., 2000; Fraige et al., 2008; Cleary, 2008; Wachs et al., 2012) or in CFD-DPM simulations (Hilton et al., 2010). An important influencing value in DPM simulations is the drag force model. Fully-resolved simulations are a useful tool to obtain such closures. In this study we extend our immersed-boundary code for spherical particles to (sphero-)cylindrical particles and we compute the flow in random static arrays thereof. Namely we compare results for the drag force with available literature data for spherical and non-spherical data.

IMMERSED BOUNDARY METHOD

Immersed boundary methods have become increasingly popular in the past two decades. An common feature of those methods is that a fixed, non-body fitted mesh is used to solve the equations that describe the motion of the fluid phase, where the immersed boundary is introduced in these equations by a body force $\boldsymbol{f}^{\mathrm{IB}}$. Several different methods have been proposed in the literature, e.g. Peskin (2002), Höfler and Schwarzer (2000), Fadlun et al. (2000), Sharma and Patankar (2005), Uhlmann (2005) and Taira and Colonius (2007). Our implementation follows the ideas of Uhlmann (2005) and we give a short description in the following. Details of the implementation and validation can be found in Kriebitzsch (2011).

Flow solver

We model incompressible, isothermal flow with constant fluid properties, described by the Navier-Stokes equation:

$$\rho_G \left(\frac{\partial}{\partial t}\boldsymbol{u} + \boldsymbol{\nabla} \cdot \boldsymbol{uu} \right) = -\boldsymbol{\nabla} P + \mu \Delta \boldsymbol{u} + \boldsymbol{f}^{\mathrm{IB}}, \qquad (1)$$

and the continuity equation:

$$\boldsymbol{\nabla} \cdot \boldsymbol{u} = 0. \qquad (2)$$

Equations (1) and (2) are solved using finite-differences on a staggered Cartesian mesh and a fractional-step method is used to compute the flowfield $\boldsymbol{u}$ and the pressure field P. Semi-implicit discretisation in time is used with explicit second-order Adams-Bashforth scheme for the convective stress term and Crank-Nicholson scheme for the viscous stress term. Central differences in space are used for all terms except the convective stresses, which are discretised by a second order minmod flux-limiting scheme.

Immersed objects

The immersed object is represented by a set of points attached to its surface. For each of these marker points a force density $\boldsymbol{F}^{\mathrm{IB}}$ is computed from the known surface velocity of the particle and an interpolated fluid velocity that has been obtained by solving equation (1) with $\boldsymbol{f}^{\mathrm{IB}} = 0$. A so-called regularized delta function is used to interpolate the fluid velocity as well as to compute the Eulerian force density $\boldsymbol{f}^{\mathrm{IB}}$ from the force at the marker points $\boldsymbol{F}^{\mathrm{IB}}$. Note that due to the spreading of the force $\boldsymbol{F}^{\mathrm{IB}}$, the effective location of the surface of a particle is smeared out slightly and the effective size of a particle is a little larger than defined by the location of the marker points. The smearing of the interface could be considered a disadvantage compared to a "sharp" representation of the interface, however the use of a regularized delta function greatly reduces the oscillations in the force and torque if the particle moves with respect to the grid (Breugem, 2012). For spherical particles the difference between the effective diameter and the diameter that defines the location of the marker points is typically 0.5 - 0.6 times the grid size.

DRAG FORCE ON A SINGLE CYLINDER

First we study the slow flow around a single (sphero-)cylinder, with the superficial velocity $\boldsymbol{U}$ parallel to the orientation of the cylindrical particle. The particle has a diameter D and a length L, as definied in figure 1.

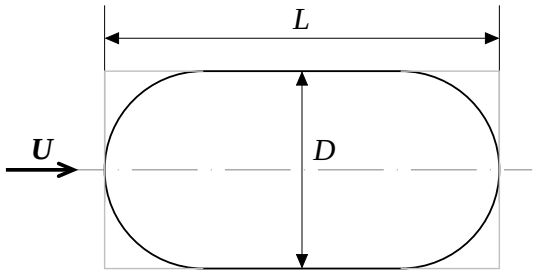

Figure 1: 2D sketch of the (sphero-)cylinder. The (sphero-)cylinder has diameter D and length L. The superficial velocity $\boldsymbol{U}$ is in direction parallel to the orientation of the (sphero-)cylinder.

Commenly used quantities to characterize non-spherical particles are

- the diameter of the volume-equivalent sphere d, defined by
$$\frac{\pi}{6} d^3 = V_{\mathrm{P}}, \qquad (3)$$
with V_{P} the volume of the particle,
- and the sphericity ψ of the particle, defined as:
$$\psi = \frac{\pi d^2}{S_{\mathrm{P}}}, \qquad (4)$$
with S_{P} the surface area of the particle.

It is convenient to define the ratios

$$x = \frac{L}{D}, \quad \xi = \frac{d}{D}. \qquad (5)$$

For a cylinder respectively a sphero-cylinder, it can be readily evaluated that

$$\xi = \begin{cases} \left(\frac{3}{2}x\right)^{1/3} & \text{for cylinders} \\ \left(\frac{3}{2}x - \frac{1}{2}\right)^{1/3} & \text{for sphero-cylinders.} \end{cases} \qquad (6)$$

The sphericity ψ is

$$\psi = \begin{cases} \frac{\pi d^2}{\pi DL + \frac{\pi}{2}D^2} = \frac{\xi^2}{x + \frac{1}{2}} & \text{for cylinders} \\ \frac{\pi d^2}{\pi DL} = \frac{\xi^2}{x} & \text{for sphero-cylinders.} \end{cases} \qquad (7)$$

The lowest-order estimate of the drag is that of a volume-equivalent sphere, therefore the dimensionless drag force F is defined as the total gas-solid interaction force divided by the Stokes drag of a volume-equivalent sphere, viz.

$$F = \frac{\boldsymbol{F}_{g \to s}}{3\pi \mu d \boldsymbol{U}}, \qquad d = \text{diameter volume-equivalent sphere} \qquad (8)$$

Note that in literature it is custom to use a $K = 1/F$. To our knowledge there are unfortunately no theoretical results for finite (sphero-)cylinders in finite systems, only for infinitely long cylinders in finite systems, and finite cylinders in unbounded systems. Happel and Brenner (1983) have derived the following expression for the drag force on an infinitely long cylinder in a dilute square array, where the flow is parallel to the cylinder:

$$F_{\mathrm{L}} = \frac{\boldsymbol{F}_{g \to s}}{4\pi \mu \boldsymbol{U} L} = \frac{1}{-\ln\phi - 1.5 + 2\phi - \frac{1}{2}\phi^2} \qquad (9)$$

with ϕ the volume fraction. This force thus diverges for an unbounded fluid. Note that Drummond and Tahir (1984) adjusted the coefficient from 1.5 to 1.476336. Gluckman et al. (1972) and Youngren and Acrivos (1975) have formulated the problem of slow flow past finite-length cylinders in an unbounded fluid in terms of linear integral equations, the solution of which is then obtained numerically by reducing the equations to a systems of linear algebraic equations. The results are given in table 1. Experimental correlations are usually constructed for very general systems, aimed to fit a wide range of non-spherical particles (discs, cylinders, plates, spheroids) and general flow direction (cross-wise and length-wise). For Stokes flow, Heiss and Coull (1952) have given the following empirical relation:

$$\log F = \frac{0.27(\xi - 1)}{\xi^{0.345}\psi^{1/2}} - \log\left(\xi \psi^{1/2}\right) \qquad (10)$$

Hölzer and Sommerfeld (2008) have recently suggested the following correlation, which also holds for inertial flow:

$$\begin{aligned} F &= F_o + F_1 \mathrm{Re}^{1/2} + F_2 \mathrm{Re} \text{ with} \\ F_o &= \frac{2}{3}\frac{1}{\psi} + \frac{1}{3}\frac{1}{\psi_\perp}, \\ F_1 &= \frac{1}{8}\frac{1}{\psi^{3/4}}, \\ F_2 &= \frac{0.0175}{\psi_\perp} 10^{0.4(-\log\psi)^2}. \end{aligned} \tag{11}$$

with $\psi_\perp$ ratio of the projected cross-section areas of the volume-equivalent sphere and of the particle, projected on the plane perpendicular to the flow. The Reynolds number is defined as $\mathrm{Re} = \rho_G d U/\mu$. The general accuracy of such correlations is not high: the average accuracy of (11) is in the range of 20%, while the maximum deviation is around 70%. However, one should keep in mind that they are applicable to a wide range of particles.

Simulations using the IB method

The flow around a single (sphero-)cylinder in a periodic box is computed, so that effectively an infinite regular array is simulated. The box was nearly rectangular, the dimension in the length-wise direction of the cylinder being slightly larger. The particle moves with a constant velocity and a body force is added to the equations of motion for the fluid (1) such that there is no net momentum flux into the system.

Although it is custom to work in dimensionless units for these type of simulations, the basic quantities were set in SI units, and equal to those of air: fluid viscosity $\mu = 1.5 \cdot 10^{-5}$ Pa.s, fluid density $\rho_G = 1\,\mathrm{kg/m^3}$. The time step and grid size of the fluid solver were set to $\Delta t = 10^{-5}$s, $h = 5 \cdot 10^{-5}$m. The effect of the time step has been tested for two systems ($L/D = 2$ and $L/D = 4$ at a solid volume fraction of $\phi = 0.0201716$). Reducing the time step by a factor of 2 gave results that were around 1% larger, which is below the general margin of error of the method.

With respect to the grid size, it is not the absolute value that is relevant, but rather the value relative to the particle size, i.e. the resolution that is used to solve the flow around the object. Computations have been performed with two resolutions: $D' = 10$ grid cells, and $D' = 20$ grid cells, where D' is the diameter that is used to set the marker point for the IB method. The resolution for the length scales accordingly, i.e. when $L/D = 4$ then $D' = 10$ grid cells implies that L' = 40 grid cells. Since it was found for spheres that the true diameter was typically half a lattice spacing larger than the one that was used to set the marker points, it is assumed that the same was true for cylinders. Hence, the actual diameter D and length L, which are the ones that are used in all subsequent analysis (calculation of volume equivalent sphere diameter d, volume fraction ϕ) was chosen to be half a lattice spacing larger, i.e. $D = D' + 0.5h$, $L = L' + 0.5h$; Note that the true x is then equal to the ratio $L/D = (L' + 0.5h)/(D' + 0.5h)$, however $x = L'/D'$ is taken (which take the precice values 2, 4, and 10); the differences are of the order of a 2-4 % for the lowest resolution, and 1-2 % for the highest resolution. It will be seen later that the differences in the drag force for high and low resolution are small, so this slight difference is not an issue.

Finally, the superficial velocity $\boldsymbol{U}$ at which the particles are moving into the length-wise direction was set such that the particle Reynolds number (calculated with D) was equal to 0.1, i.e. the Stokes flow regime.

Comparison of the simulation data with results from theory and experiment

In order to compare with the theoretical result for an infinite domain by Gluckman et al. (1972) and Youngren & Acrivos (1975), the data has to be extrapolated to $\phi = 0$. For spheres, the relation between the drag force F_{SC} in a dilute SC array, and the drag force F_∞ in an unbounded fluid is given by Hasimoto's expression (Hasimoto, 1959):

$$F_{\mathrm{SC}} = \frac{F_\infty}{1 - 1.7601\phi^{1/3} + \phi - 1.5593\phi^2 + \ldots}$$

(Note that for spheres the normalized drag force $F_\infty = 1$ by construction). We now make the assumption that this functional form, to order ϕ, holds for all particles which have a moderate aspect ratio. That is, one assumes that for a cylinder in a periodic domain, the relation between F_{SC} and F_∞ is given by

$$F_{\mathrm{SC}} = \frac{F_\infty}{1 + \alpha\phi^{1/3} + \phi \ldots} \tag{12}$$

with α an unknown parameter. Equation (12) can be written as

$$\frac{1}{F_{SC}(1+\phi)} = \frac{1}{F_\infty} + \frac{\alpha}{F_\infty} \cdot \frac{\phi^{1/3}}{1+\phi}$$

So when plotting the data for the drag force obtained from the simulations as $(F_{SC}(1+\phi))^{-1}$ *vs.* $\phi^{1/3}/(1+\phi)$, the data should fall on a straight line, where the intersection with the y-axis is equal to $1/F_\infty$. In figure 2 the data is shown in this representation. From the figure it is clear that there is no effect of the grid-size resolution.

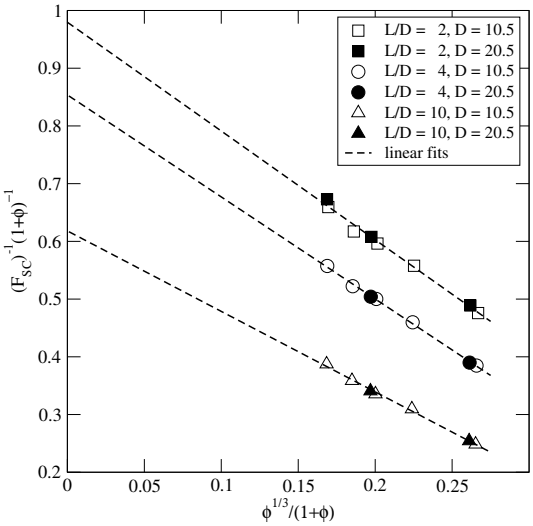

Figure 2: Simulation data for the drag force for different aspect ratios in a periodic array. In this representation, the intersection of the linear fit with the y-axis provides an estimate for the inverse of the normalized drag force for a single cylinder in an unbounded system.

The values F_∞ that follow from a linear fit through the data are given in table 1, together with the theoretical data by Gluckman et al. (1972) and Youngren and Acrivos (1975), and the experimental results by Heiss and Coull (1952).

L/D	Simulation	Theory		Experiment	
	This work (fig. 2)	*Youngren & Acrivos*	*Gluckman et al*	*Heiss & Coull*	*Hölzer & Sommerfeld*
2	1.021	1.0235	1.0142	0.786	0.801
4	1.171	1.0730	1.0764	0.946	0.909
10	1.618	1.2690	1.1947	1.852	1.151

Table 1 Predictions for the normalized drag force F on a cylinder in an unbounded fluid from simulation, theory and experiment.

Excellent agreement with the theoretical result by Youngren & Acrivos for $L/D = 2$ is found, however not so for the higher aspect ratios. This is understandable, because the corrections that were made for the effect of the periodic images was "borrowed" from the Hasimoto expression valid for spheres. Since for infinitely long cylinders the correction actually diverges as $\phi \to 0$ (see equation (9)), one may expect that the convergence will go slower as L/D gets larger, and that the leading order term in the denominator of equation (12) will be different from $\phi^{1/3}$.

It would be more appropriate for $L/D = 10$ to compare the result for $F_{\mathrm{L}} = \boldsymbol{F}_{g\to s}/4\pi\mu L\boldsymbol{U}$ (which is the force per unit length, non-dimensionalized by $4\pi\mu U$) with expression (9) for an infinitely long cylinder. Note that in that case, one should use the 2-D solid volume fraction $\phi_{2D} = \frac{1}{4}\pi D^2/(L_x L_y)$ in (9). The simulation results for F_{L} as a function of ϕ_{2D} are shown in figure 3, together with the prediction from (9). It can be seen that indeed the data approaches the theoretical result for the infinite cylinder as L/D gets larger, and that in particular the dependence on ϕ is very similar.

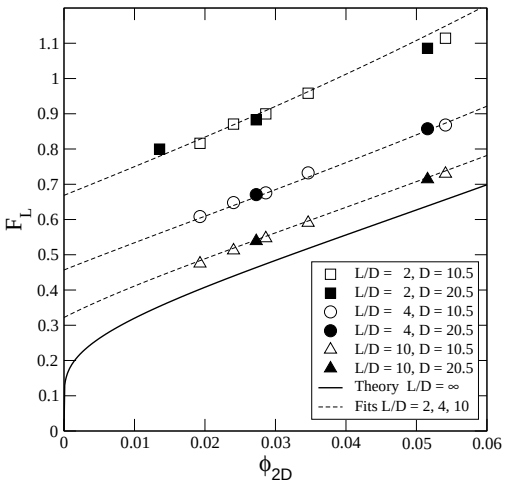

Figure 3: Simulation data for the force on a single cylinder at different aspect ratios in a periodic array. The drag force is normalized by $4\pi\mu LU$, so that F_{L} represents the non-dimensionalized force per unit length. The solid line is the theoretical result for a cylinder of infinite length, given by equation (9). The dashed lines are calculated from equation (13).

An *ad hoc* fit to the simulation data is given by

$$F_{\mathrm{L}} = \frac{1}{-\ln(\phi + 1/(10x)) - 1.5 + 2\phi} \tag{13}$$

Interestingly, for an unbounded fluid ($\phi = 0$), expression (13) reduces to $F_{\mathrm{L}} = 1/(\ln(10x) - 1.5)$. For $x = 10$ this gives $F_{\mathrm{L}} = 0.322$, which corresponds to $F = 1.31$, which is within 3% of the Youngren & Acrivos result (see table 1) for a cylinder with $L/D = 10$ in an unbounded fluid.

DRAG FOR DENSE ARRAYS OF RANDOMLY ORIENTED CYLINDERS

For dense arrays, such as shown in figure 4, it is useful to make the connection between the drag force and the pressure drop, since the latter can be directly measured in experiments of packed beds, and can also be estimated from a Carman-Kozeny analysis.

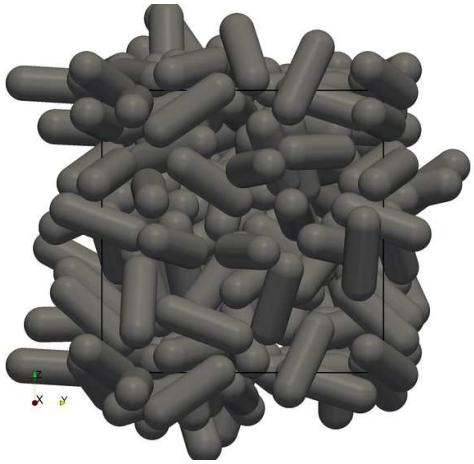

Figure 4: Example of a random periodic array of 100 sphero-cylinders with an aspect ratio $x = \frac{L}{D} = 3$.

It can be readily shown that for flow past an array of identical particles, the relation between the *average* gas-solid interaction force on a particle $\boldsymbol{F}_{g\to s}$ and the pressure drop ∇P is

$$\boldsymbol{F}_{g\to s} = -\frac{1}{\phi} V_{\mathrm{p}} \nabla P$$

with V_{p} the volume of the particle. For (sphero)-cylinders $V_{\mathrm{p}} = \pi d^3/6$, hence one gets the following relation between the average normalized drag force F as defined by (8) and the pressure drop:

$$F = -\frac{1}{\phi}\frac{d^2}{18\mu U} \cdot \nabla P \tag{14}$$

Carman-Kozeny analysis

The Carman-Kozeny analysis gives that the pressure drop for flow through a porous medium is set by the hydraulic radius r_h, defined as the ratio of the free volume in the pores to the "wet" surface area. For a system of N identical, but arbitrary shaped particles with volume V_{p} and surface area S, r_h is equal to

$$\begin{aligned} r_h &= \frac{V_{\mathrm{tot}} - NV_{\mathrm{p}}}{NS} = \frac{(1-\phi)}{\phi}\frac{V_{\mathrm{p}}}{S_{\mathrm{p}}} = \frac{1-\phi}{\phi} \cdot \frac{\frac{1}{6}\pi d^3}{S_{\mathrm{p}}} \\ &= \frac{1-\phi}{6\phi} \cdot \frac{\pi d^2}{S_{\mathrm{p}}} d = \frac{1-\phi}{6\phi} \cdot \psi d \end{aligned} \tag{15}$$

with ψ defined by (4). When using a Kozeny constant of 5, the permeability becomes

$$\kappa = \frac{(1-\phi)r_h^2}{5} = \frac{(1-\phi)^3}{180\phi^2}(\psi d)^2 \tag{16}$$

so that the pressure drop is:

$$-\nabla P = \frac{1}{\kappa}\mu U = 180 \cdot \frac{\phi^2}{(1-\phi)^3}\frac{\mu U}{(\psi d)^2} \tag{17}$$

which is the well-known Carman equation, only with a diameter ψd instead of the usual diameter of the sphere. Inserting this into (17), and using the relation (14) between the normalized average drag force and the pressure drop, yields

$$F = 10\frac{\phi}{(1-\phi)^3}\cdot\frac{1}{\psi^2} \qquad (18)$$

with ψ the sphericity, given by (7). So the normalized drag force is modified by a factor ψ^{-2} compared to the drag force for a dense array of spheres at the same packing.

Experimental results

Nemec and Levec (2005) have measured the pressure drop for particles of different shape to a generalized Ergun equation, which already takes the non-sphericity into account by using a diameter ψd as follows from the Carman-Kozeny theory (e.g. see (17)):

$$-\nabla P = A\cdot\frac{\phi^2}{(1-\phi)^3}\frac{\mu U}{(\psi d)^2} + B\cdot\frac{\phi}{(1-\phi)^3}\frac{\rho_G U^2}{(\psi d)} \qquad (19)$$

The original Ergun coefficients A and B take the values 150 and 1.75, whereas the Carman-Kozeny analysis using a Kozeny constant of 5 gives $A = 180$. Nemec & Levec have fitted the pressure drop data for cylinders to (19), where the results for A are shown in table 2[1]:

ψ	x	Exp.	(20)
0.874	1.0	200	183
0.874	1.0	180	183
0.866	1.33	210	186
0.835	1.91	210	196
0.782	2.94	240	217
0.722	3.81	230	244
0.672	5.77	250	272

Table 2 Value for the Ergun coefficient A (rounded values) as obtained from experiments, and calculated from expression (20).

It can be seen that for higher x, the data deviates significantly from both 150 and 180, indicating the use of a diameter ψd in the Ergun or Carman equation is not sufficient to capture the effect of having non-spherical particles; in other words, according to the experiments, the Carman-Kozeny assumption that for Stokes flow r_h is solely determining the permeability seems to break down, and an additional correction is required. Nemec & Levec have fitted the data to the following functional form, using the coefficients 150 and 1.75 as a basis:

$$A = \frac{150}{\psi^{3/2}}, \qquad B = \frac{1.75}{\psi^{4/3}}. \qquad (20)$$

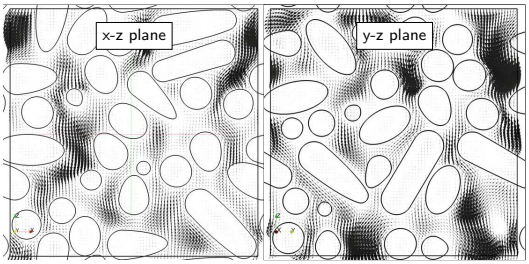

Figure 5: Slices through the central x-z plane and y-z plane of the particle bed shown in figure 4. The fluid velocity flow field and the particles are shown.

Simulation results

The set-up of the simulations was similar as described in the previous section for a single cylinder, but now for an array of sphero-cylinders with random orientation. All the particles move with the same constant velocity and a body force is added to the Navier-Stokes equation (1) such that there is no net momentum flux into the system and the relative superficial velocity $\boldsymbol{U}$ is equal to the velocity of the particles $\boldsymbol{v}$.

system parameters				simulation result			
x	ψ	N	ϕ	F	ΔF	A	ΔA
2	0.921	100	0.7004	338.3	9.3	198.3	5.4
2	0.921	300	0.7005	337.9	3.3	197.9	1.9
3	0.840	100	0.6713	299.2	11.0	201.0	7.4
3	0.840	300	0.6729	297.8	6.9	196.7	4.6
4	0.779	100	0.6422	226.7	14.0	176.6	10.9
4	0.779	300	0.6501	269.8	9.4	194.2	6.8

Table 3 Results for the average normalized gas-solid force F for a dense, random array of sphero cylinders. The coefficient A is defined by (21).

In order to create the configurations, a Monte-Carlo algorithm with overlap detection for sphero-cylinders was used. The systems contained 100 or 300 particles, and the L/D ratios of 2, 3 and 4. Periodic boundary conditions are used. A resolution of 10 grid cells was used for the diameter of the cylinder. As in the case of a single cylinder, the actual dimensions of the cylinder were taken half a lattice spacing larger. To increase the statistical accuracy, the drag force was evaluated for 10 different configurations of each system, and the value for F as presented below is the calculated as the average over these 10 results, where the error in the results is estimated from the standard deviation. The results are given in table 3.

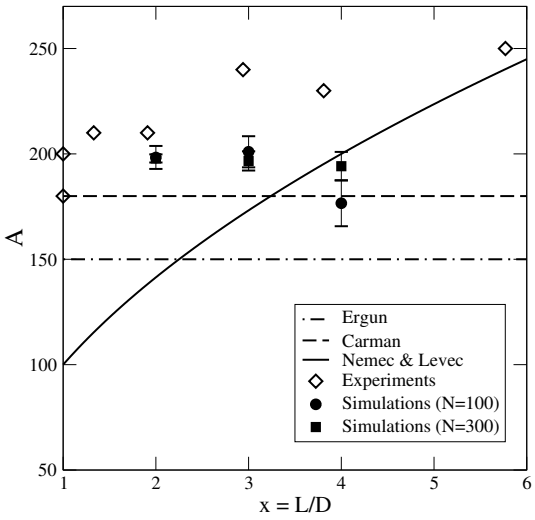

Figure 6: Results for A from experiment (cylinders) and simulations (sphero-cylinders), compared with the predictions from the Carman-Kozeny theory, the Ergun equation, and the modified Ergun equation (Nemec & Levec, see (20)).

In order to compare with the experimental data, the results for the coefficient A are shown, which is defined by the relation:

$$F = \frac{A}{18}\frac{\phi}{(1-\phi)^3}\cdot\frac{1}{\psi^2} \qquad (21)$$

[1]Note Nemec & Levec define $\psi^3 = 36\pi V^2/S^3$, with V the volume and S surface area of the object. This is equivalent to definition (4).

In the Carman-Kozeny approximation (see (18)), $A = 180$; the Ergun equation predicts $A = 150$, whereas Nemec & Levec predict that $A = \frac{150}{\psi^{3/2}}$. In figure 6 the various results for A are compared. The simulation data shows that the value of A is nearly constant, which implies Carman-Kozeny type behavior, that is, the drag force varies with $\frac{1}{\psi^2}$. Only the coefficient isabout 10 % larger than the "standard" value of 180. The experimental value is slightly larger, and seems to increase with L/D.

CONCLUSIONS AND OUTLOOK

Some first results for drag force on sphero-cylinders from fully resolved simulations were presented, in the limit of Stokes flow. Comparison of the simulation data for a single cylinder with available theoretical results is not straightforward. In the simulations both the system and the cylinder are finite, while the theoretical results are for an infinitely long cylinder in a finite system, or for a finite-length cylinder in an infinite system. Increasing the box size in the simulation and extrapolating the result to infinite dilution is hindered by the fact that for higher aspect ratios the convergence gets slower, and the precise functional form is not known as in the case of spheres. However, the analysis suggests that the simulation results are consistent with the available theoretical predictions.

For dense systems of randomly oriented sphero-cylinders the simulation data indicates that a Carman-Kozeny description, where the drag force is determined solely by the hydraulic radius, is still valid, only with a Kozeny constant that is slightly larger ($\sim$ 10%) than the usual value of $k = 5$; for lower aspect ratios this is consistent with the experimental data; for higher aspect ratios, the experiments predict a drag force that is typically 20 % larger compared to the data. It has to be stressed that these results are preliminary, and that much more extensive simulations have to be performed in order to come to any definite conclusions. In future work, also the effect of fluid inertia on the drag force will be considered. Of particular interest is also the deviation of the drag force on an individual cylinder with the average drag such as follows from a Carman-Kozeny analysis. One may expect that there will be a spreading in the force similar to what was found for spheres. However, in addition one may also anticipate a dependency of the individual force on the orientation of the cylinder with respect to the flow. If this could be adequately parametrised, it could mean a significant step forward in the modelling of gas-particle drag in DP-type simulations of non-spherical particles.

ACKNOWLEDMENTS

The authors wants to thank Marjolein Dijkstra from the University of Utrecht for providing us with the configurations of densely packed sphero-cylinders. The financial support of the European Research Council under its Advanced Investigator Grant scheme, contract number 247298 (MultiscaleFlows), and also the Netherlands Organisation for Science (NWO) is gratefully acknowledged.

REFERENCES

BREUGEM, W.P. (2012), "A second-order accurate immersed boundary method for fully resolved simulations of particle-laden flows", *Journal of Computational Physics*, **231**, 4469–4498.

CLEARY, P. (2008), "The effect of particle shape on simple shear flows", *Powder Technology*, **179**, 144–163.

DRUMMOND, J. and TAHIR, M. (1984), "Laminar viscous flow through regular arrays of parallel solid cylinders", *International Journal of Multiphase Flows*, **10**, 515–540.

FADLUN, E., VERZICCO, R., ORLANDI, P. and MOHD-YUSOF, J. (2000), "Combined immersed-boundary finite-difference methods for three-dimensional complex flow simulations", *Journal of Computational Physics*, **161**, 35–60.

FRAIGE, F., LANGSTON, P. and CHEN, G. (2008), "Distinct element modelling of cubic particle packing and flow", *Powder Technology*, **186**, 224–240.

GLUCKMAN, M., WEINBAUM, S. and PFEFFER, R. (1972), "Axisymmetric slow viscous flow past an arbitrary convex body of revolution", *Journal of Fluid Mechanics*, **55**, 677–709.

HAPPEL, J. and BRENNER, H. (1983), Low Reynolds number hydrodynamics, Martinus Nijhoff Publishers, The Hague.

HASIMOTO, H. (1959), "Periodic solutions of the stokes equations", *Journal of Fluid Mechanics*, **5**, 317–328.

HEISS, J. and COULL, J. (1952), "The effect of orientation and shape on the settling velocity of non-isometric particles in a viscous medium", *Chemical Engineering Progress*, **48**, 133–140.

HILTON, J., MASON, L. and CLEARY, P. (2010), "Dynamics of gas-solid fluidised beds with non-spherical particle geometry", *Chemical Engineering Science*, **65**, 1584–1596.

HÖFLER, K. and SCHWARZER, S. (2000), "Navier-stokes simulation with constraint forces: Finite-difference method for particle-laden flows and complex geometries", *Physical Review E*, **61**, 7146–7160.

HÖLZER, A. and SOMMERFELD, M. (2008), "New simple correlation formula for the drag coefficient of non-spherical particles", *Powder Technology*, **184**, 361–365.

KRIEBITZSCH, S. (2011), "Direct numerical simulation of dense gas-solid flows", Ph.D. thesis, Eindhoven University of Technology.

NEMEC, J. and LEVEC, J. (2005), "Flow through packed bed reactors: 1. single-phase flow", *Chemical Engineering Science*, **60**, 6947–6957.

PESKIN, C. (2002), "The immersed boundary method", *Acta Numerica*, **11**, 479–517.

SHARMA, N. and PATANKAR, N. (2005), "A fast computation technique for the direct numerical simulation of rigid particulate flows", *Journal of Computational Physics*, **205**, 439–457.

TAIRA, K. and COLONIUS, T. (2007), "The immersed boundary method: A projection approach", *Journal of Computational Physics*, **225**, 2118–2137.

UHLMANN, M. (2005), "An immersed boundary method with direct forcing for the simulation of particulate flows", *Journal of Computational Physics*, **209**, 448–476.

VAN DER HOEF, M., VAN SINT ANNALAND, M., DEEN, N. and KUIPERS, J. (2008), "Numerical simulation of dense gas-solid fluidized beds: A multiscale modeling strategy", *Annual Review of Fluid Mechanics*, **40**, 47–70.

VU-QOUC, L., ZHANG, X. and WALTON, O. (2000), "A 3-D discrete-element method for dry granular flows of ellipsoidal particles.", *Computer Methods in Applied Mechanics and Engineering*, **187**, 483–528.

WACHS, A., GIROLAMI, L., VINAY, G. and FERRER, G. (2012), "Grains3D, a flexible DEM approach for particles of arbitrary convex shape – part I: Numerical model and validation", *Powder Technology*, **224**, 374–389.

YOUNGREN, G. and ACRIVOS, A. (1975), "Stokes flow past a particle of arbitrary shape: A numerical method of solution", *Journal of Fluid Mechanics*, **69**, 377–403.